Emulated Inertia Control for the Stand-Alone Microgrid with High Penetration of Renewable Energy Sources

Ratnam Kamala Sarojini*, K. Palanisamy**‡

* School of Electrical Engineering, Research Scholar, Vellore Institute of Technology, Vellore, Tamil Nadu, India

**School of Electrical Engineering, Associate Professor, Vellore Institute of Technology, Vellore, Tamil Nadu, India

(kamala.rtnm@gmail.com, kpalanisamy@vit.ac.in)

‡ School of Electrical Engineering; Vellore Institute of Technology, Vellore, Tamil Nadu, India,

kpalanisamy@vit.ac.in

Received: 16.05.2020 Accepted:05.06.2020

Abstract- The gradual increase in power generation from renewable energy sources (RES), results in a reduction in power system inertia. It adversely affects the stable operation of the microgrids that contains high penetration of RES. The frequency stability concerns caused by the penetration of RES in the grid-connected system is controlled by synchronous generator (SG). Whereas in the stand-alone microgrid, which entails of RES deteriorates the frequency stability under power imbalances. The emulated inertia control (EIC) technology used for the power electronic inverter mimics the inertia of SG. EIC provides an effective solution for power systems with low inertia. This paper analyses the performance of EIC applied to the stand-alone microgrid that comprises of RES only. The utilization of EIC in stand-alone microgrid successfully addresses the frequency stability issues under solar irradiation and load variations. Furthermore, the small-signal stability analysis of the EIC is performed to analyze the stability under parameter variation. The simulation analysis shows that the frequency response and DC bus voltage is regulated in sudden disturbances with EIC efficiently as compared with constant voltage constant frequency (CVCF). The proposed EIC strategy is tested and compared with CVCF using the hardware in the loop (HIL) simulation with the help of real-time simulator OP5700 to verify the feasibility.

Keywords Inertia emulation, virtual inertia, stand-alone microgrid, frequency control, constant voltage constant frequency control.

Nomenclature

P_{Set}	Active power reference
P_{Cal}	Active power output
Q_{Set}	Reactive power reference
Q_{Cal}	reactive power output
D_P	Dropping coefficient of frequency

D_q	Dropping coefficient of voltage
J	Inertia
k	Constant
ω	Angular frequency of the system
ω_r	Angular frequency reference
V_m	Output voltage of the system
V_m^*	Reference voltage
$\dot{\omega}_{s,\max}$	Rate of change of frequency (ROCOF)

1. Introduction

Power systems are changing from a centralized few large SG's to a relatively large number of distributed generation based on RES with electronic power converters [1]. The microgrid has emerged as with the rise in RES power generation growth. The microgrid can function as two types based on the connection, i.e. the grid-connected mode and the stand-alone mode. The increase in the number of power electronic converters between RES and grid affects the system stability due to lack of inertia [2], [3]. Due to SG's inherent synchronization capability and inertia, electricity generation is dominated by SG in the traditional power system. Hence, the system stability is maintained by the SG in the grid-connected microgrid. Whereas in the stand-alone microgrid, which entails of RES deteriorates the frequency stability under power imbalances [4], [5]. In a stand-alone microgrid, it is necessary to maintain the frequency and voltage magnitude at acceptable limits. The allowed frequency deviation is ± 1.5Hz and allowed maximum ROCOF ($\dot{\omega}_{s,\max}$) is 0.6 Hz/s for the safe and secure operation of stand-alone microgrid.

In a stand-alone microgrid, an SG-based diesel generator uses droop control technique to generate the reference frequency and voltage magnitude. However, a pattern of this control strategy follows that of a traditional power system [6]. The droop control technique was initially introduced for the uninterruptible power supply system, which supplies local loads. The active power-frequency (P-f) droop control was used for the stand-alone microgrid in [7]. In [8],[9] the P-V droop controller has been used for reactive power sharing in the stand-alone microgrid. In [10], the detailed small-signal modelling of the droop controller for the microgrid was developed. The droop control based stand-alone microgrid provides small, or no inertia that leads to frequency stability issues. The low inertia stand-alone microgrid results in large frequency deviations and high ROCOF under significant load transitions leads to tripping of RES and loads. An appropriate control approach is required to employ inertia in the stand-alone microgrid, with a significant share of renewable power generation. Therefore, the implementation of inertia emulation control methods to power electronic inverter places a vital role in the frequency stability of stand-alone microgrid.

Various approaches have been recommended to address these low-inertia problems, like adding of rotational devices or deployment of synchronous condensers to power system [11]. On the other hand, emulating the inertia to the power electronic converters was studied in [12]–[15]. An evolving concept implemented to support the inertia is known as EIC. In [12], the complete mathematical model of the SG is taken to design the inertia emulation algorithm, but it results in numerical instability. In [16], the second-order model of SG is considered to design the control algorithm; here, the calculation of ROCOF leads to complexity in the algorithm. The EIC control scheme is an appropriate solution to the low inertia power system. The EIC mimics the SG characteristics, by regulating the switching pattern of the inverter to offer the virtual inertia and to decrease frequency nadir during disturbances. In [17], the small-signal modelling of EIC with ideal grid-connected inverter is analyzed. The implementation of the EIC algorithm in the power system is reported in [18]. The use of inertia emulation in the microgrid is analyzed in [19]. Inertia emulation using hybrid energy storage consists of battery and supercapacitor for the single-phase rooftop system is proposed in [20]. However, earlier investigation on EIC only emphasis on the controller design, grid-connected applications and hardly discussed the application of EIC in the stand-alone microgrid.

The frequency stability of stand-alone microgrid under load transitions is to be examined inevitably. In [21], the author used the virtual synchronous generator in the stand-alone microgrid based on gas engine generator to mimic the inertia. In [22], the author used the inertia emulation controller to emulate the inertia for the wind turbine. In [23], energy storage is used to control the frequency of islanded microgrid, consisting of wind-solar generating stations. In [23]–[25], proved that the utilization of energy storage in the isolated microgrid improves the frequency under power imbalance with constant voltage and constant frequency control (CVCF). However, the inertia is not an inherent capability in CVCF control. Due to the lack of inertia in CVCF control, the frequency deviations are more.

In previous studies, the performance analysis of EIC and CVCF in stand-alone microgrids that consisting of photovoltaic generators and energy storage device is hardly reported in the literature. The main objective of this paper is the application of the EIC approach in a stand-alone microgrid to utilize the energy from the battery to provide inertia to the stand-alone microgrid. EIC control able to reduce the frequency nadir and can improve the stability without losing the performance of other MPPT control algorithm for source variations and load fluctuations. The small-signal analysis of EIC is performed to evaluate the stability of EIC under inertia and damping coefficient variations. A comparison of the stability parameters like frequency and DC bus voltage is carried out with the EIC over CVCF under load transition. The transient performance of the system with EIC and CVCF are analyzed under sudden load transitions by using HIL experimental setup.

The rest of this paper is organized as follows. Section 2 describes the structure of stand-alone microgrid, section 3 explains the core concept of EIC, CVCF and DC voltage controller, section 4 describes the small-signal modelling of EIC, section 5 deals with the simulation results, section 6 describes the HIL results and the conclusion is given in section 7.

2. System Configuration

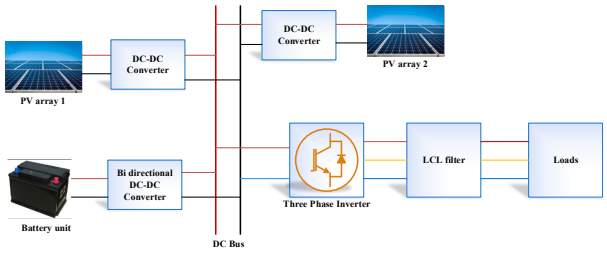

Fig. 1. Structure of Stand-alone microgrid.

A typical stand-alone microgrid under this study consists of two photovoltaic (PV) arrays, battery unit, three-phase inverter and loads are shown in Fig. 1. The boost converter is used to connect the PV arrays to the DC bus. It is used to extract the available amount of power from PV arrays by utilizing maximum power point tracking technique. The three-phase inverter converts the DC to AC, and it is coupled to the load with LCL filter. The LCL filter aims to remove high switching frequency components from the inverter current. The battery, along with bi-directional converter is attached to the DC bus to balance the load.

The system conFig.d in this work consists of three modules. The following section describes each module in the framework.

- PV arrays and dc-dc converters.
- Battery unit with bidirectional DC-DC converters.
- Three-phase inverter with LCL filter.

2.1. PV arrays and dc-dc converters

The two PV arrays of 5 kW of power generation capacity are considered in this work. One of the PV unit with dc-dc converter is shown in Fig. 2. These two PV arrays are coupled to the DC bus through boost converters. The boost converter uses a basic P & O control technique to extract the available power from PV units. The P & O control technique adjusts the voltage and examines whether power is increased or not. If the power extracted from the PV array is not improved, then the operating voltage is not changed.

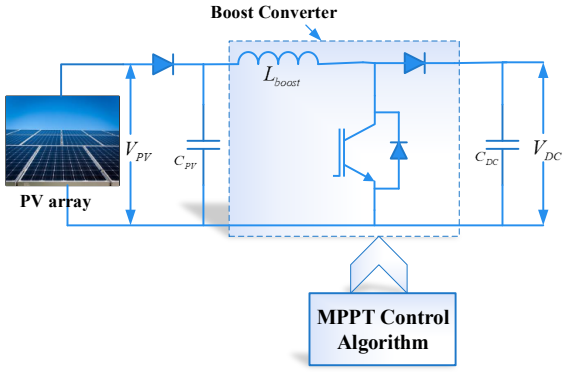

Fig. 2. PV unit with dc-dc converter.

2.2. Battery unit with bidirectional DC-DC converter

The PV arrays are working on MPPT, does not take care of sudden load variations, and it affects the stability of the microgrid. Sudden change in either demand or generation (due to irradiance fluctuations) in stand-alone microgrid can create more frequency deviations and ROCOF. The battery is included in the system to maintain the stability of stand-alone microgrid. The battery, along with bi-directional converter is attached to the DC bus to balance the load, as shown in Fig. 3. The battery in the system has to respond to the frequency imbalances. The switching pulses for the bi-directional converter are generated from the dc voltage controller discussed in section 3.

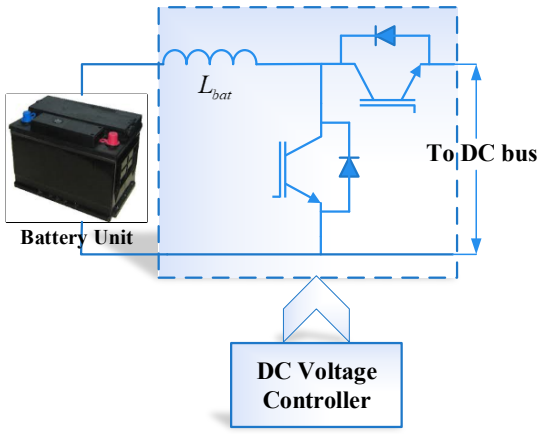

Fig. 3. Battery unit with Bi-directional converter.

2.2.1. *Energy Storage Requirement for the stand-alone microgrid*

This section estimates the size of the battery to balance the power mismatch and to maintain frequency stability. It is essential to control the state of charge of the battery in allowable range:

$$SOC_{\min} \le SOC \le SOC_{\max} \quad (1)$$

In this work, the energy storage capacity of the battery is assessed by using [26]–[28]:

$$\Upsilon I_{rated}(\frac{t}{60}) = (\text{Ah}) * \text{k} \quad (2)$$

Where Υ is the portion of the rated load current. I_{rated} is the rated load current, t is the time duration that the battery offers power into the system, k - a fraction that defines the average discharge/charge current of the battery.

In this paper, the battery storage is assumed to provide 40 per cent of the total load current (Υ=0.4) over a 5 h time duration. Hence, Ah rating of the battery for the given system is calculated to be 15 Ah.

2.3. *Three-phase inverter with LCL filter*

Fig. 4 shows the three-phase inverter, which used to connect to the DC bus with three-phase loads through the filter. The filter is designed to reduce harmonic content [29]. The switching pulses of the three-phase inverter are generated using the EIC is discussed in section 3.

The EIC applied to the inverter used to alter the load angle for balancing power under load transitions to decrease the frequency nadir. The battery used to handle both inertia response and primary frequency regulation of the considered system. The detail description of the DC voltage controller of the battery and EIC of the inverter is discussed in the following section.

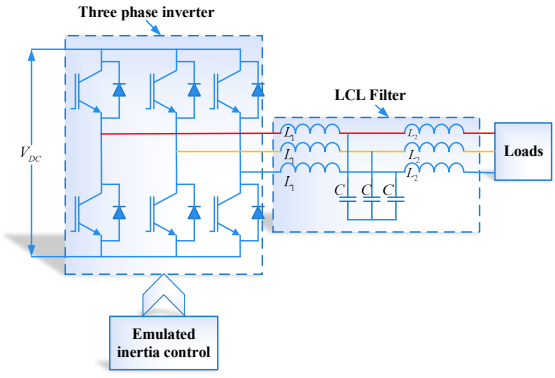

Fig. 4. Three-phase inverter with LCL filter.

3. Control Description

This section explains controllers used in this paper such as emulated inertia control, constant voltage constant frequency control and DC voltage controller.

3.1. *Proposed emulated inertia control for stand-alone microgrid*

EIC enhances frequency stability of the power system and allows more power generation from renewables into the system [30]. EIC uses the swing equation to emulate the inertia. EIC resembles the SG characteristics to enhance the frequency stability. Moreover, it emulates inertia to the power electronic inverter like SG to support frequency stability of stand-alone microgrid. The control diagram for the EIC is illustrated in Fig. 5. The main concept of EIC is to calculate the extra power required for the frequency deviation and to add this extra power to set point. The EIC responds to frequency variations and alters the load angle. The electrical appearance of both EIC and SG mathematically equivalent. Hence, the inertial response of the EIC is similar to the SG.

The EIC developed based on the swing equation to alter the load angle of the inverter θ. The fundamental concept of EIC is shown in (3)-(5).

$$(P_{Set} - P_{Cal}) / \omega - D_P(\omega - \omega_r) = J\frac{d\omega}{dt} \quad (3)$$

$$\frac{d\theta}{dt} = \omega \quad (4)$$

$$\frac{1}{k}\int (Q_{Set} - Q_{Cal}) + D_q(\mathrm{V}_m^* - V_m)dt = E \quad (5)$$

The EIC is divided into two control parts. The first part of EIC is used to alters the load angle based on the frequency deviation. The damping term for the given frequency deviation is included to the difference in the set torque (calculated with set power) to the torque output (calculated with output power). The integrator, along with inertia term alters the load angle based on the difference in torque terms. Whereas in the second part of EIC regulates the voltage amplitude. Depends on the reactive power variation, the voltage amplitude can be altered. The voltage amplitude and the load angle are combined to get the reference voltage for the inverter. The reference voltage generated by the EIC is fed to PWM to produce the pulses for the inverter. Whenever there is a change in the demand, the EIC alters the load angle to inject/absorb the power with the help of energy stored in the battery. Implementation of EIC in a stand-alone microgrid reduces the frequency deviations and ROCOF.

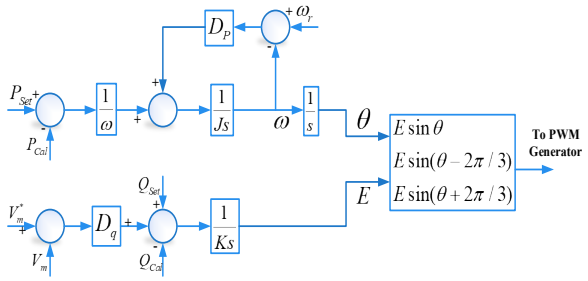

Fig. 5. Emulated inertia control.

3.2. Conventional constant voltage constant frequency control technique

The conventional CVCF control technique for the inverter is displayed in Fig. 6. The PI controller is used to provide the reference voltage amplitude as an output with the voltage amplitude error as an input. The integrator is used to calculate the angle with a reference frequency. Here, the 50 Hz is considered as the constant frequency for the operation of microgrid with CVCF control. The reference voltage is given to the PWM generator to produce the switching pulses. The frequency of the microgrid with CVCF control is compared with the EIC control under load variations. The purpose of including CVCF technique in this paper is to evaluate and compare the performance with EIC. The qualitative comparison of EIC and CVCF controllers are present in Table 1.

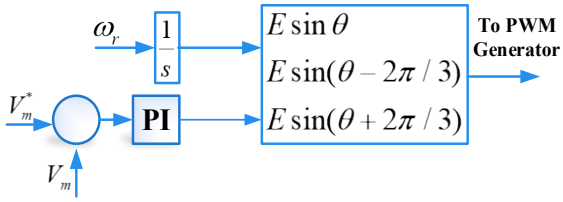

Fig. 6. CVCF Control diagram.

Table 1. Qualitative comparison of CVCF and EIC controllers

	CVCF control	EIC Control
Inertia control	No	Yes
Frequency control	No	Yes
Voltage control	No	No
Plug and play	Cannot	Can

3.3. DC Voltage controller of stand-alone microgrid

The DC voltage controller at the battery has to operate properly to achieve frequency stability by using EIC. The DC bus voltage must be preserved constant to accomplish power balance in the system. The DC voltage controller produces the reference current to be injected/drawn into/from the DC bus to preserve the DC bus voltage constant. The control algorithm applied to the bi-directional converter of the battery is shown in Fig. 7.

$$v_e(t) = v_{dc}^*(t) - v_{dc}(t) \tag{6}$$

$$i_b^*(t) = k_{p1} v_e(t) + k_{i1} \int v_e(t) dt \tag{7}$$

Where k_{p1} and k_{i1} are the PI controller gains, $i_b^*(t)$ is the battery reference current, $v_{dc}^*(t)$ is the reference DC bus voltage, $v_{dc}(t)$ is the measured DC bus voltage, $v_e(t)$ is the DC bus voltage error and I_b is the battery current.

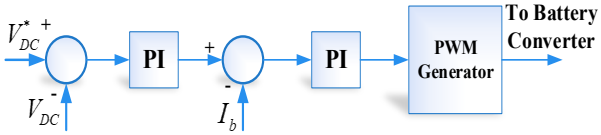

Fig. 7. DC voltage control of stand-alone microgrid.

The DC bus voltage V_{DC} is compared to reference DC bus voltage V_{DC}^*, as indicated in Eq. (6), and the error is fed to PI control. The PI control generates the battery reference current as shown in Eq. (7), then it is compared to the battery current. Depends on the error in the battery current the PI controller alters the duty ratio. Thereby the DC bus voltage is maintained constant, and the required power is injected/absorbed to/from the system.

4. Small-Signal Modelling and Parameter Design of EIC

This section analyses the small-signal stability and parameter design of EIC. The small-signal modelling of EIC is shown in Fig. 8.

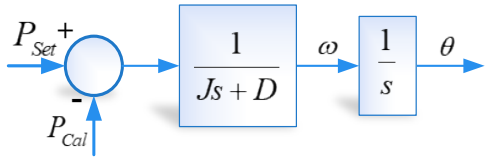

Fig. 8. Small-signal modelling of emulated inertia control.

The Eq. (3) of EIC is rewritten in terms of load angle:

$$P_{Set} - P_{Cal} = J\omega\frac{d^2\theta}{dt^2} + D_P\omega\frac{d\theta}{dt} \quad (8)$$

The active power output (P_{Cal}) can be written as

$$P_{Cal} = \frac{EV}{X}\sin\theta \quad (9)$$

The Eq. (8) can be transformed as for the rotor angle difference to the power imbalance is

$$\frac{\Delta\theta}{\Delta P} = \frac{1}{(J\omega)s^2 + (D_P\omega)s + (\frac{EV}{X})} \quad (10)$$

Therefore, the roots of Eq. (10) are defined by equating the characteristic equation to zero is known as:

$$s_{1,2} = \frac{-D_P \pm \sqrt{(D_P^2 - 4J\omega EV / X)}}{2J\omega} \quad (11)$$

The Eq. (11) proved that the poles are complex conjugate and lies in left half of s-plane. Thus, EIC is critically stable in nature. The poles do not encompass k and D_q, which means that the parameter design of active power loop is independent of reactive power loop. To design the EIC in stable manner, the imaginary portion of Eq. (11) must equate to zero. Then, the critical inertia (J_c) can be known as:

$$J_c = \frac{D_P^2 X}{4\omega EV} \quad (12)$$

The system operates in the underdamped state if inertia value J is chosen as more than J_c, then the natural frequency of oscillation and damping ratio can be given as

$$\omega_n = \sqrt{\frac{3EV}{2J\omega X}} \quad (13)$$

$$\xi = D_P\sqrt{\frac{X}{6J\omega EV}} \quad (14)$$

The natural frequency of oscillation is dependent on inertia (J) and reactance (X). Whereas the damping ratio depends on the damping coefficient (D_P), inertia (J) and reactance (X).

4.1. Design Guideline for drooping coefficient (D_P)

The drooping coefficient(D_P) is designed in such a way that the angular frequency (ω) is in the acceptable range. The drooping coefficient is decided by using (15).

$$D_P \geq \frac{P_{\max} - P_{\min}}{\omega_{\max} - \omega_{\min}} \quad (15)$$

Where $P_{\max}$ is the maximum active power capacity of the system, $P_{\min}$ is the minimum active power generated by the system, $\omega_{\max}$, $\omega_{\min}$ are the maximum and minimum allowable angular frequency by the system.

4.2. Parameters influence in ROCOF

The ROCOF protection relays of generating units may be activated by a rapid return of frequency after the contingency event [31]. The ROCOF of the system must be smaller than the allowable ROCOF limit ($\dot{\omega}_{s,\max}$).

ROCOF of the system after the contingency event can be calculated by rearranging Eq. (3):

$$ROCOF = \frac{P_{resrve} - D_P\omega_s}{J} < \dot{\omega}_{s,\max} \quad (16)$$

Where $P_{resrve} = P_{Set} - P_e$, $\omega_s \in [\omega_r - \omega_{\max}, \omega_r - \omega_{\min}]$, $P_{resrve} \in [P_{Set} - P_{\max}, P_{Set} - P_{\min}]$. The ROCOF reaches to a maximum value when the large power imbalance occurs. According to Eq. (16), D_P and J must be selected effectively to reduce ROCOF value must be in the allowable range.

4.3. Parameter analysis of EIC using pole-zero map

The pole distribution with different values of D_P , J and X are shown in Fig. 9. Fig. 9(a) illustrates that poles are slowly approaching to the imaginary axis as the J alue is increasing. If J is increasing further the system state changes from the underdamped to the overdamped. As J increasing system damping and natural frequency of oscillations decreased, and overshoot increased. Fig. 9(b) indicates that the system characteristic roots intersect at one point and transform to complex roots as D_P decreases. The damping of the system improves with D_P . The overshoot and settling time of the power decreases with D_P increasing. The reactance X has an influence on the natural frequency of oscillations, which has no effect on damping coefficient. If X decreases, the system damping decreases and response speed increases. The pole-zero map for variations in reactance X is shown in Fig. 9(c).

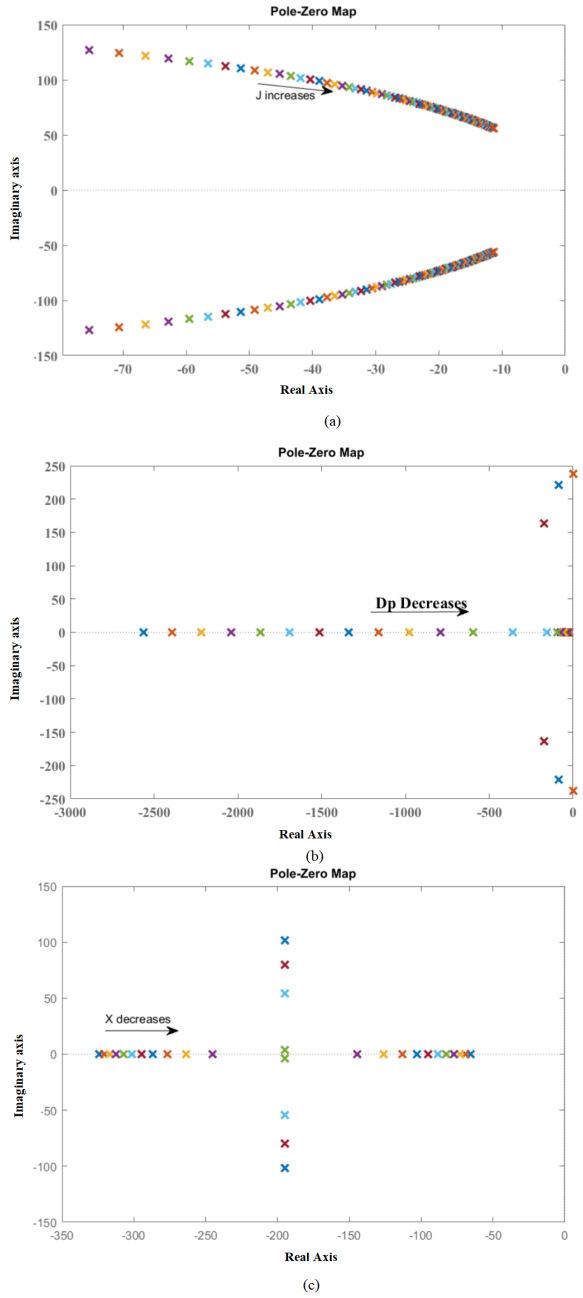

Fig. 9. Pole-Zero map (a) for variation in J , (b) For Variations in D_P (c) For Variations in X .

5. Simulation Results

The simulations are carried out using the Matlab/Simulink environment. Two PV arrays, battery unit, three-phase inverter and loads are considered in these simulations as per Fig. 1. The detailed simulation parameters are tabulated in Table 2. This section further divided into two parts. The first part of the section deals with the performance of the EIC under parameter variation of inertia (J) and drooping coefficient (D_P). Last part of the section proves the effectiveness of the EIC control over the CVCF control under sudden variations in load.

Table 2. Qualitative comparison of CVCF and EIC controllers

Parameters	Values
Reference frequency (f)	50 Hz
Reference Voltage (V^*)	220 V
Rated DC bus voltage (V_{DC})	500 V
PV cell	$V_{OC} = 37.3$ V, $I_{SC} = 8.2$ A, $V_m = 30.3$, $I_m = 7.5$, $N_S = 15$, $N_P = 2$.
Rating of battery unit	15 Ah
Battery terminal voltage	250 V
DC bus Capacitor	3300 μF
Inverter side inductance (L_1)	2.1 mH
Load side inductance (L_2)	0.8 mH
Filter capacitance (C)	12 μF
Frequency Drooping Coefficient (D_P)	50
Inertia coefficient (J)	0.058 Kg.m^2
Voltage drooping coefficient (D_q)	120
Gain (k)	1000 A. s
PI coefficients of CVCF control	0.5,22

5.1. Performance validation under parameter variation

Initially, the stand-alone microgrid operates with a load of 8000W. After that, another load of 4000 W is connected to the system at 2 s. The drooping coefficient and inertia are playing a vital part to enhance the stability. Several simulations are carried out to understand the impacts of the parameters (D_P and J) on the performance of EIC. The system shown in Fig. 1 is simulated with J = 0.058 and D_P = 75. Later the inertia remains unaltered, and the drooping coefficient is changed from 75 to 100 and 150. The frequency takes a lesser time to settle, and the oscillations are less as the D_P increases under load transition as depicted in Fig. 10(a).

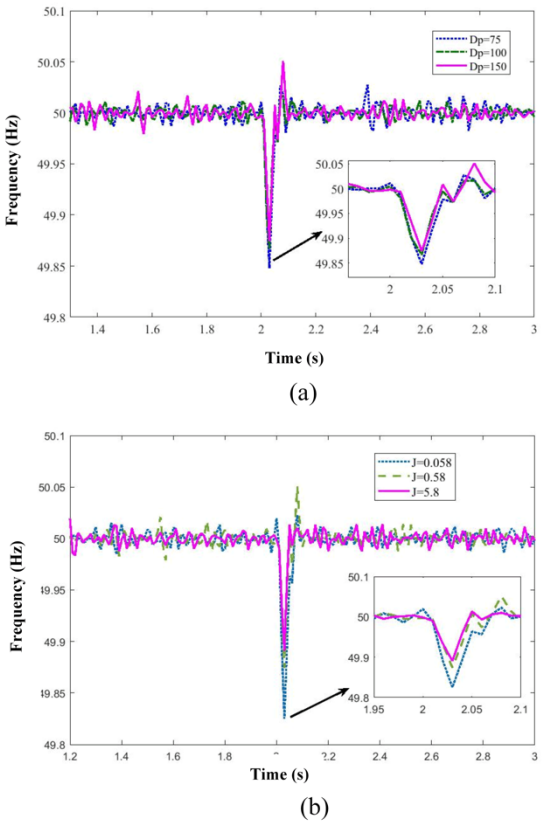

Fig. 10. Frequency under Parameter variation (a)Varying D_P (b)Varying J.

When D_P value rises the overshoot and settling time is decreased, and this can suppress the oscillations of frequency and enhances the stability, and it is illustrated in Fig. 10(a). The system frequency is shown in Fig. 10(b) for different values of the inertia parameter. In this scenario, the inertia parameter is changed from J=0.058 to 0.58 and 5.8. From Fig. 10(b), when J increases, the frequency nadir decreases, peak time and settling time of frequency increases.

Table 3 summarizes the frequency nadir and ROCOF for different values of drooping coefficient (D_P) and inertia (J). From Fig. 10 and Table 3, it is concluded that as the drooping coefficient (D_P) and inertia (J) values are increasing the frequency nadir and ROCOF decreases.

Table 3. Comparison of frequency and ROCOF for different parameter values

Frequency Drooping coefficient (D_P)	Inertia (J)	Frequency nadir	ROCOF
75	0.58	49.847	0.193
100	0.58	49.863	0.1813
150	0.58	49.874	0.176
75	0.058	49.824	0.228
75	5.8	49.89	0.146

5.2. Comparison of EIC over CVCF

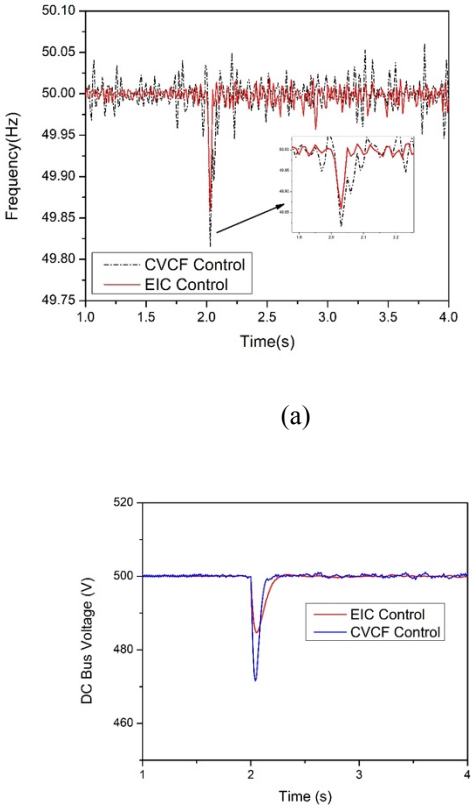

Fig. 11. Comparison of CVCF control and EIC Control under load change ;(a) Frequency (b) DC bus voltage.

This section compares the performance of the EIC with CVCF under load transition. The system parameters like frequency and DC bus voltage are compared with both the controllers (EIC and CVCF). The frequency deviation and the frequency oscillations are more due to the lack of inertia in the CVCF control. Whereas the inertia is emulated from the SG in EIC control, then the frequency deviation is less. The frequency deviates more with CVCF control than the EIC control under load transition as shown in Fig. 11. Similarly, the DC bus voltage is also deviating to 473V with CVCF control and 485V with EIC control. Fig. 11 concluded that as compared with the CVCF control, the EIC control limits both the frequency and DC bus voltage deviations.

Table 4 summarizes the frequency nadir, DC bus voltage and ROCOF for both the controllers (EIC and CVCF). From Fig. 11 and Table 4, it concluded that the frequency nadir, DC bus voltage deviation, ROCOF are less in case of EIC as compared with CVCF. The EIC approach for the stand-alone microgrid enhances the stability under load transitions.

Table 4. Performance comparison of EIC and CVCF controllers

Controller	Frequency nadir	ROCOF	DC bus voltage
EIC Control	49.89	0.146	484.61
CVCF Control	49.795	0.234	473.5

6. HIL results

The performance of EIC in stand-alone microgrid was investigated in HIL simulations. The stand-alone microgrid displayed in Fig. 1, EIC and CVCF controllers were dumped to the OP5700 real-time simulator to observe the frequency variations. The system parameter values used in HIL are similar to those used in simulation studies.

6.1. Under load transition

In this case, the stand-alone microgrid with CVCF control and EIC control is tested for constant irradiance with step increase and step decrease in load power. The full power 5000 W of each PV array is produced at an irradiance of 1000 W/m^2. The load of 8000 W is connected to the system initially, and the extra power produced from both the PV arrays is stored in battery. Fig. 12 illustrates that the power from inverter, battery, PV array1, PV array2, frequency and DC bus voltage with CVCF control in load transitions. Fig. 13 illustrates that the power from inverter, battery, PV array1, PV array2, frequency and DC bus voltage with EIC control in load transitions. At $t = t_1$ s another load of 4000W is added, the deficient power in the system is supplied by the battery. The sudden increase in load demand creates the deviation in frequency and DC bus voltage.

Usually in traditional power system with SG, the kinetic energy resides in the rotor is used to reduce ROCOF and frequency deviation under load transitions. Similarly, the EIC increases the load angle to supply the power whenever the frequency deviates from the nominal value. Hence, the frequency deviations are less with EIC control because it is emulating the inertial characteristics of SG. Due to lack of inertial behavior in CVCF control frequency deviations are more. The frequency dip and voltage dip are more in case of CVCF control as compared to the EIC control. At $t = t_2$ s, 4000W load is removed, and the excess power is stored in the battery. The EIC controller triggers whenever frequency deviated from the nominal value. The EIC alters the load angle to balance the frequency. When the load angle decreases the DC bus voltage increases, then the DC voltage controller activates to charge the battery. The EIC controller and DC bus voltage controller activate until the system reaches power balance.

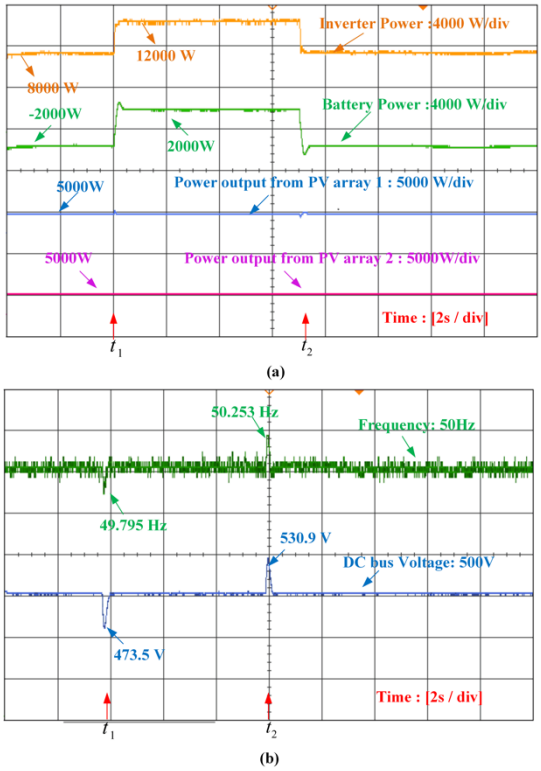

Fig. 12. Load transition under constant irradiation with CVCF control (a) power from inverter, battery, PV array1, PV array2; (b) frequency and DC bus voltage.

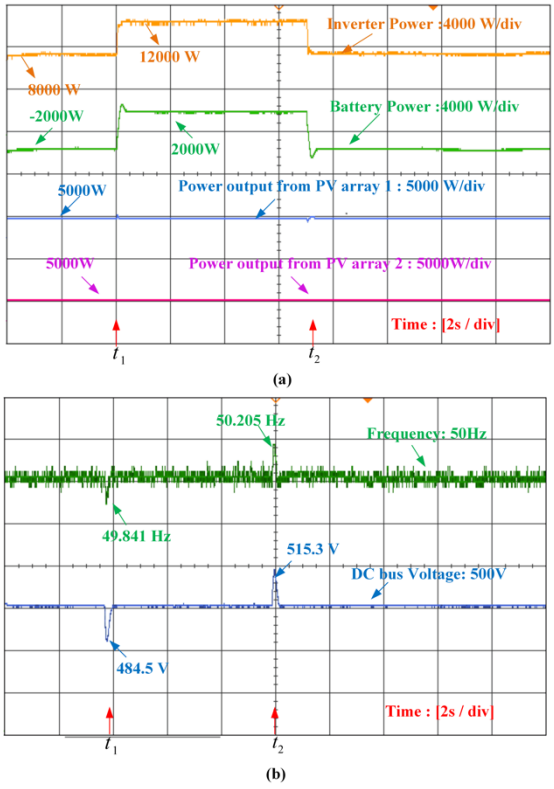

Fig. 13. Load transition under constant irradiation with EIC control (a) power from inverter, battery, PV array1, PV array2; (b) frequency and DC bus voltage.

Whereas in CVCF control the frequency rise is more due to lack of inertia. The battery used to balance the demand and PV generation in the stand-alone microgrid under sudden load variations. However, the frequency and DC bus voltage deviations are more with CVCF control as compared with the EIC control under load transitions.

6.2. Under PV power variation

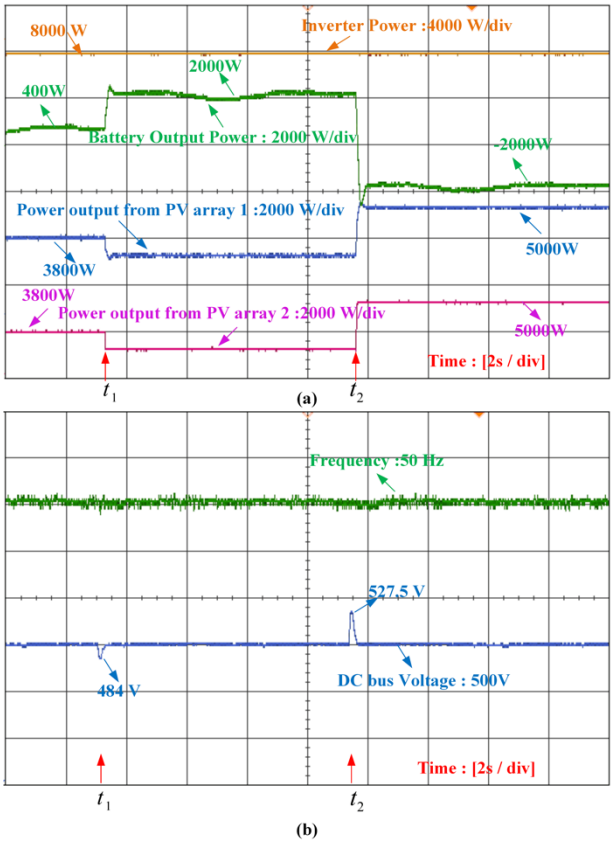

Fig. 14. Real power variations at constant Load with CVCF control (a) Inverter output power, Battery power, the output power of PV array1, the output power of PV array2; (b) Frequency and DC bus voltage.

In this scenario, the stand-alone microgrid with CVCF The sudden decreasing of the PV power creates the reduction in DC bus voltage and does not create the deviation in frequency. In this transition, there is no effect of frequency observed, but DC bus voltage is reduced more when compared with EIC control. At $t = t_2$ s, the PV power generated from both PV arrays are increased suddenly with irradiation level. The excess power generated from the PV arrays is absorbed by the battery. This transition creates the increase in DC bus voltage and does not create effect on the frequency. The deviation in DC bus voltage is more with CVCF control compared to EIC control. As compared to CVCF control, the EIC control effectively worked to mitigate the frequency deviation and to maintain the DC bus voltage under load variations and irradiation variations also.

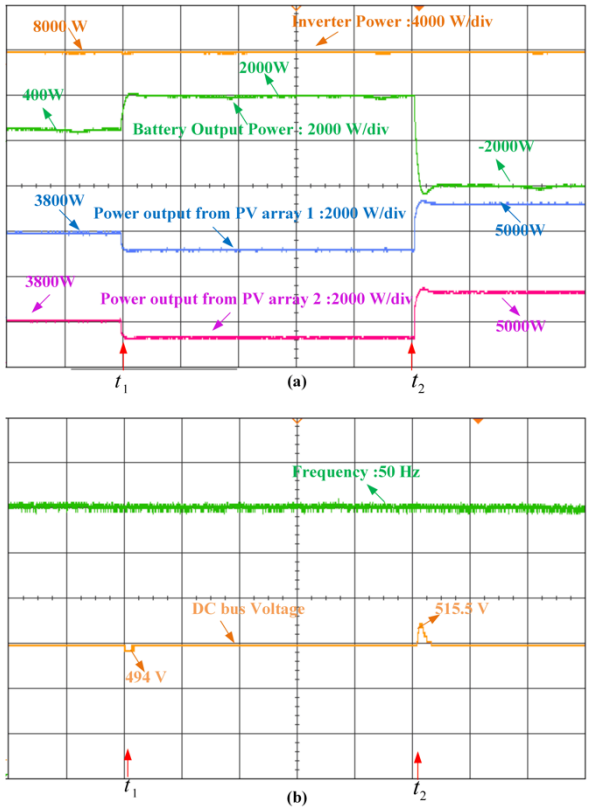

Fig. 15. Real power variations at constant load with EIC control (a) Inverter output power, Battery power, the output power of PV array1, the output power of PV array2; (b) Frequency and DC bus voltage.

7. Conclusion

The stand-alone microgrids that comprise only RES are lack of system inertia and predominantly affecting the stability of stand-alone microgrid. The utilization of EIC emulates the inertia of an SG to handle with sudden power fluctuations. Whereas the battery is utilized to store/absorb the power to balance the generation and demand. For stable operation of the system, the EIC alter the load angle to inject/absorb the active power to limit the frequency deviation. The battery is supplying/absorbing the power in the inertial response with EIC. The small-signal stability analysis carried out in this paper proved that the EIC could provide sufficient inertial response with proper selection of damping coefficient and inertia. The performance comparison of EIC and CVCF controllers was presented. Both the HIL and simulation results proved that the EIC has better performance over the CVCF control in the stand-alone microgrid. Hence, an EIC controller can enhance the transient response of frequency and DC bus voltage in the stand-alone microgrid system under variations in solar irradiation and load.

Acknowledgements

Authors like to acknowledge the funding agencies for the supported received for this project activities by Grant Project No. SR/FST/ETI-420/2016(C)) “Fund for Improvement of S&T infrastructure in Universities & Higher Educational

Institutions (FIST)" Department of Science and Technology (DST)– Government of India. Funded to establish the PHIL set-up which is a part of this research project.

References

[1] H. Bevrani, T. Ise, and Y. Miura, "Virtual synchronous generators: A survey and new perspectives," Int. J. Electr. Power Energy Syst., vol. 54, pp. 244–254, January 2014.

[2] X. Zhu, Z. Xie, S. Jing, and H. Ren, "Distributed virtual inertia control and stability analysis of dc microgrid," IET Gener. Transm. Distrib., vol. 12, pp. 3477–3486, May 2018.

[3] M. S. U. Zaman, S. B. A. Bukhari, R. Haider, M. O. Khan, and C. H. Kim, "Effects of modified inertia constant and damping coefficient on power system frequency response," Int. J. Renew. Energy Res., vol. 9, pp. 525–531, March 2019.

[4] K. S. Ratnam, K. Palanisamy, and G. Yang, "Future low-inertia power systems: Requirements, issues, and solutions - A review," Renew. Sustain. Energy Rev., vol. 124, pp. 109773, February 2020.

[5] S. Sakurai, O. Sakamoto, and T. Nitta, "Linearized model of power system with synchronous generator, variable renewable energy generation and load," 8th Int. Conf. Renew. Energy Res. Appl. *ICRERA 2019*, Brasov, pp. 276–279, November 2019.

[6] J. Tang, B. Xiong, Y. Li, Y. Qiu, C. Yuan, and Y. Sun, "An optimized decentralized control strategy of grid-connected residential photovoltaic inverters based on voltage sensitivity matrix," 8th Int. Conf. Renew. Energy Res. Appl. ICRERA 2019, Brasov pp. 69–74, November 2019.

[7] DE. Olivares, A. Mehrizi-Sani, AH . Etemadi, CA .Cañizares, R. Iravani, M. Kazerani, AH . Hajimiragha, O. Gomis-Bellmunt, M. Saeedifard, R. Palma-Behnke, GA. Jiménez-Estévez "Trends in microgrid control," IEEE Trans. Smart Grid, vol. 5, no. 4, pp. 1905–1919, May 2014.

[8] Y. Li and Y. W. Li, "Power management of inverter interfaced autonomous microgrid based on virtual frequency-voltage frame," IEEE Trans. Smart Grid, vol. 2, no. 1, pp. 18–28, January 2011.

[9] E. Kurt and G. Soykan, "Performance analysis of DC grid connected PV system under irradiation and temperature variations," 8th Int. Conf. Renew. Energy Res. Appl. ICRERA 2019, Brasov, pp. 702–707, November 2019.

[10] K. Yu, Q. Ai, S. Wang, J. Ni, and T. Lv, "Analysis and Optimization of Droop Controller for Microgrid System Based on Small-Signal Dynamic Model," IEEE Trans. Smart Grid, vol. 7, no. 2, pp. 695–705, November 2016.

[11] D. Byrne, "All Island Tso Facilitation of Renewables Studies," *EirGrid*, 2013. [Online]. Available: http://www.eirgridgroup.com/site-files/library/EirGrid/All-Island-SiemensPTI-WP1-091109-part1.pdf. [Accessed: 08-May-2019].

[12] Y. Chen, R. Hesse, D. Turschner, and H. Beck, "Dynamic Properties of the Virtual Synchronous Machine (VISMA)," Proc. ICREPQ 11, vol. 1, pp. 755–759, Las Palmas de Gran Canaria (Spain) April 2011.

[13] Q. C. Zhong, P.-L. P. Nguyen, Z. Ma, and W. Sheng, "Self-synchronised Synchronverters: Inverters without a Dedicated Synchronisation Unit," IEEE Trans. Power Electron., vol. 29, no. c, pp. 1–1, April 2014.

[14] P. Rodriguez.,C. Citro, JI. Candela,J. Rocabert, A. Luna "Flexible Grid Connection and Islanding of SPC-Based PV Power Converters," vol. 3, no. c, pp. 2690–2702, February 2018.

[15] K. Visscher and S. de Haan, "Virtual synchronous machines (VSG's) for frequency stabilisation in future grids with a significant share of decentralized generation," SmartGrids Distrib. 2008. IET-CIRED. CIRED Semin., no. 0118, pp. 1–4, June 2008.

[16] T. Loix, S. Breucker, P. Vanassche, J. Van den, J. Driesen, K. Visscher, "Layout and Performance of the Power Electronic Converter Platform for the VSYNC Project," IEEE Bucharest Power Tech Conf., Bucharest,pp. 1–8, June 2009.

[17] K. sarojini Ratnam and P. Kaliannan, "Small Signal Modelling and Determination of Critical Value of Inertia for Virtual Synchronous Generator," Innov. Power Adv. Comput. Technol., India, pp. 1–6, March 2019.

[18] J. Fang, H. Li, Y. Tang, and F. Blaabjerg, "Distributed Power System Virtual Inertia Implemented by Grid-Connected Power Converters," IEEE Trans. Power Electron., vol. 33, pp. 8488–8499, December 2017.

[19] K. Shi and H. Ye, "Virtual Inertia Control Strategy in Microgrid Based on Virtual Synchronous Generator Technology," IEEE Access, vol.6, no. c, pp. 27949–27957, May 2018.

[20] RK.Sarojini, K. Palanisamy, P. Sanjeevikumar, "Inertia emulation control technique-Based frequency control of grid-connected single-phase rooftop photovoltaic system with battery and super-capacitor," IET Renew. Power Gener., vol. 7, pp. 1156-1163, December 2019.

[21] H. S. Hlaing, J. Liu, Y. Miura, H. Bevrani, and T. Ise, "Enhanced Performance of a Stand-Alone Gas-Engine Generator Using Virtual Synchronous Generator and Energy Storage System," IEEE Access, vol. 7, pp. 176960–176970, December 2019.

[22] Y. Ma, W. Cao, L. Yang, F. F. Wang, and L. M. Tolbert, "Virtual Synchronous Generator Control of Full Converter Wind Turbines with Short-Term Energy Storage," IEEE Trans. Ind. Electron., vol. 64, no. 11, pp. 8821–8831, 2017.

[23] G. Delille, B. François, and G. Malarange, "Dynamic frequency control support by energy storage to reduce the impact of wind and solar generation on

isolated power system's inertia," IEEE Trans. Sustain. Energy, vol. 3, no. 4, pp. 931–939, August 2012.

[24] J. H. Lee, S. H. Lee, and S. K. Sul, "Variable-speed engine generator with supercapacitor: Isolated power generation system and fuel efficiency," IEEE Trans. Ind. Appl., vol. 45, no. 6, pp. 2130–2135, September 2009.

[25] A. Mondal, A. A. Renjit, M. S. Illindala, and J. H. Eto, "Operation and impact of energy storage system in an industrial microgrid," IEEE Ind. Appl. Soc. - 51st Annu. Meet. IAS 2015, Conf. Rec., pp. 1–7, October 2015.

[26] N. Mendis, K. M. Muttaqi, and S. Perera, "Management of battery-supercapacitor hybrid energy storage and synchronous condenser for isolated operation of PMSG based variable-speed wind turbine generating systems," IEEE Trans. Smart Grid, vol. 5, no. 2, pp. 944–953, January 2014.

[27] J. Alshehri, A. Alzahrani, and M. Khalid, "Voltage and frequency control of microgrids with distributed generations and battery energy storage," 8th Int. Conf. Renew. Energy Res. Appl. ICRERA 2019, Brasov , pp. 381–385, November 2019.

[28] L. Barote and C. Marinescu, "Li-Ion energy storage capacity estimation in residential applications with EV," 8th Int. Conf. Renew. Energy Res. Appl. ICRERA 2019, Brasov , pp. 326–330, November 2019.

[29] K. H. Ahmed, S. J. Finney, and B. W. Williams, "Passive Filter Design for Three-Phase Inverter Interfacing in Distributed Generation," Compat. Power Electron., pp. 1-9, May 2007.

[30] U. Tamrakar, D. Shrestha, M. Maharjan, B. Bhattarai, T. Hansen, and R. Tonkoski, "Virtual Inertia: Current Trends and Future Directions", Applied Sciences, vol. 7, pp. 654, July 2017.

[31] J. Fang, H. Li, Y. Tang, and F. Blaabjerg, "On the Inertia of Future More-Electronics Power Systems", IEEE Journal of Emerging and Selected Topics in Power Electronics, vol.4, pp. 2130-2146, October 2018.